Research article

JHEP|Reports

Identification of a cancer stem cell-like subpopulation that promotes HCC metastasis

Authors

Chunyuan Yang, Yang Li, Zhaohai Wang, …, Jianyuan Luo, Limei Guo, Yuxin Yin

Correspondence

yinyuxin@hsc.pku.edu.cn (Y. Yin), guolimei@bjmu.edu.cn (L. Guo).

Graphical abstract

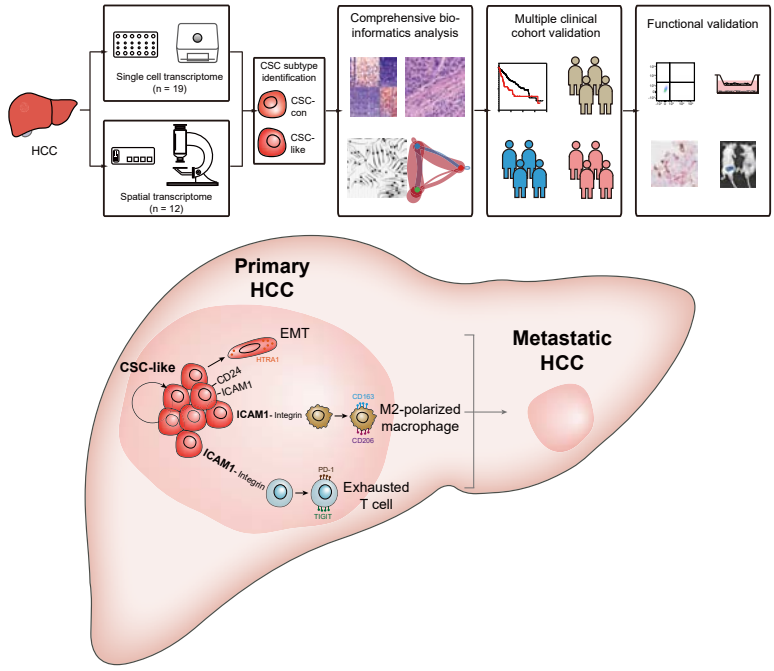

Highlights:

- Comprehensive analysis of scRNA-seq and spatial transcriptomic data was used to investigate the characteristics of HCC CSCs.
- CSC-like cells, a distinct subpopulation of CSCs, exhibited higher invasiveness compared with conventional CSCs.
- CSC-like cells were characterized by high expression levels of CD24, ICAM1, ACSL4, BAG3, C17orf67, GOLGA8B, and RBM26.
- Functional interactions between CSC-like cells and immune cells promoted an immunosuppressive microenvironment.
- Targeting ICAM1 signaling disrupted CSC-like cell-mediated immunosuppression, enhancing antitumor immune responses.

Impact and implications:

The heterogeneity of CSCs in HCC has been identified, yet the identification and characterization of metastasis-promoting CSC subpopulations remain unexplored. Here, we identified a CSC-like tumor cell subpopulation that promotes HCC metastasis by increasing cell invasiveness and suppressing antitumor immune responses via the ICAM1 signaling pathway. Our study uncovers novel mechanisms of HCC metastasis from the perspective of CSCs, and proposes potential tumor therapeutic strategies by inhibiting cellular interactions between CSC-like cells and immune cells.

https://doi.org/10.1016/j.jhepr.2024.101302

Research article

JHEP|Reports

Identification of a cancer stem cell-like subpopulation that promotes HCC metastasis

Chunyuan Yang[1,†], **Yang Li**[1,2,†], **Zhaohai Wang**[3,†], **Hui Shan**[2,†], Guangze Zhang[1], Xiangyan Meng[1], Guangxi Wang[1], Zhiyuan Hou[1], Xuyang Zhao[1], Xin Zhang[1], Anhang Liu[1], Yuntao Bing[1], Guanglin Lei[4], Yan Jin[1], Jianyuan Luo[5], Limei Guo[1,*], Yuxin Yin[1,2,*]

JHEP Reports **2025**. vol. 7 | 1–14

Background & Aims: Cancer stem cells (CSCs) are well-established drivers of tumorigenesis, but their role in regulating tumor metastasis remains poorly understood. Here, we report the identification and characterization of a cluster of metastasis-promoting CSC-like cells in hepatocellular carcinoma (HCC).

Methods: CSC-like cells in HCC were identified through the analysis of single cell RNA-sequencing data from 19 HCC samples. The stemness and invasive characteristics of these cells were evaluated using bioinformatical analyses of nine clinical cohorts and experimental validations. Spatial transcriptomics sequencing of 12 HCC samples revealed the cellular interactions between the CSC-like cells and tumor microenvironments, which were validated through gene co-expression analyses and immunohistochemistry. Finally, signaling pathway blockade was used to assess the potential clinical application of CSC-like cells.

Results: Through comprehensive analyses of single cell RNA-sequencing data from 19 patients with HCC and spatial transcriptomics data from 12 patients with HCC, a metastasis-promoting CSC-like subpopulation was identified. These CSC-like cells expressed high levels of epithelial–mesenchymal transition genes and were associated with poor prognosis of HCC. Histologically, CSC-like cells were enriched in highly aggressive tumors, especially in intrahepatic disseminated foci, where they interacted with immune cells. Functionally, CSC-like cells induced macrophage M2 polarization and T cell exhaustion through the ICAM1 signaling pathway, forming immunosuppressive microenvironments. Downregulation of ICAM1 expression in CSC-like cells suppressed macrophage M2-polarization and T cell exhaustion, thereby reversing antitumor immune effects.

Conclusions: Our study identified a metastasis-promoting CSC subpopulation, providing a potential perspective for CSC-targeted therapies in HCC.

Introduction

Primary liver cancer has as the third highest mortality rate of all human malignancies, with ~75–85% of liver cancers classified as hepatocellular carcinoma (HCC).[1,2] Tumor metastasis and recurrence are the leading cause of HCC-related death,[3] with short-term tumor recurrence closely linked to tumor metastasis.[4] Therefore, tumor metastasis represents a crucial focus in HCC treatment investigations. Unfortunately, recently developed HCC treatment strategies, including surgical resection, radiofrequency ablation, tumor embolization, and tumorigenesis-based chemotherapy drugs, have limited therapeutic effects on HCC metastasis.[5] Hence, there is an urgent need for tumor metastasis-targeted therapeutic strategies for HCC treatment.

Tumor heterogeneity, driven by cancer stem cells (CSCs), is the leading cause of treatment failure, metastasis, and recurrence.[6] CSCs are a rare population of tumor cells with self-renewing capacity that drive tumor initiation and are resistant to standard radiation and chemotherapeutic interventions.[7] Increasing evidence suggests the heterogeneity of the CSC population, with CSC subtypes identified in gastric and colorectal cancer.[8,9] Remarkably, different CSC subtypes have been shown to have different roles in tumorigenesis and metastasis. In colorectal cancer, the tumorigenesis of the primary tumor is initiated by leucine-rich repeat-containing G-protein-coupled receptor 5^+ ($LGR5^+$) CSCs, whereas metastases are driven by $LGR5^-$ CSCs.[9,10] However, the exact CSC subpopulation that initiates tumor metastasis, and the characteristics of these cells, remain elusive.

Single-cell RNA-sequencing (scRNA-seq) is a high-throughput sequencing method used to uncover gene expression profiles at a single cell resolution. However, histological information is lost during the experimental process. Spatial transcriptomics (ST) maps transcriptomics *in situ*, thereby complementing scRNA-seq.[11] The combination of

* Corresponding authors. Addresses: Institute of Systems Biomedicine, Department of Pathology, School of Basic Medical Sciences, Peking University Health Science Center, Beijing 100191, China; Tel.: +86 10 8280 5571; fax: +86 10 8280 1380 (Y. Yin); Department of Pathology, School of Basic Medical Sciences Peking University, Peking University Third Hospital, Beijing 100191, China; Tel.: +86 10 8280 2561; fax: +86 10 8280 1685 (L. Guo).
E-mail addresses: yinyuxin@hsc.pku.edu.cn (Y. Yin), guolimei@bjmu.edu.cn (L. Guo).
† These authors contributed equally.
https://doi.org/10.1016/j.jhepr.2024.101302

scRNA-seq and ST has elucidated the landscape of tumor microenvironments (TMEs) in multiple tumor types.[12–14] Nevertheless, the integration of scRNA-seq and ST has not yet been applied to the investigation of CSC. Thus, in this study, we used scRNA-seq and ST in HCC and identified a CSC-like tumor subpopulation. Unlike conventional tumorigenic CSCs, this CSC-like population exhibits distinct characteristics. Comprehensive bioinformatic analyses were used to reveal gene expression profiles, histological distribution features, and *in situ* cellular interaction networks of CSC-like cells. Experimental validation and multiple clinical cohorts were also used to confirm the functions of this cell type (Fig. 1A). Based on these strategies, we identified CSC-like cells as a metastasis-promoting subpopulation of CSCs in HCC, and uncovered the underlying mechanisms involved.

Materials and methods

Patient samples

Our study was approved by the Ethics Committee of Peking University Third Hospital (Beijing, China). All research was conducted in accordance with both the Declarations of Helsinki and Istanbul. Patients with liver cancer who underwent surgery at the Department of General Surgery of the Peking University Third Hospital were enrolled according to the following criteria: (1) pathologically confirmed HCC; (2) no history of other malignancies; and (3) no anti-cancer therapy before surgery. All patients were informed and kept anonymous.

All other information regarding the materials and methods is provided in the supplementary data online.

Results

Identification of CSC subclusters in HCC

To investigate the transcriptomes of CSCs in HCC, we performed scRNA-seq analysis on tumors and peritumoral specimens from five patients with HCC (cohort 1, Table S1). The clinicopathological information about these patients is summarized in Table S2. In addition, we integrated our scRNA-seq data with a published HCC dataset (cohort 2, Table S1),[15] which contained tumor tissues from 14 patients. Collectively, the integrated dataset comprised 116,858 single cells collected from 19 patients with HCC. We then clustered all cells into five major partitions: T/natural killer (NK) cells, stromal cells, hepatocytes, myeloid cells, and B cells (Fig. 1B). To validate the identities of these cell types, we used lineage-specific markers, including *CD3D* and *GNLY* for T/NK cells, *CD68* and *CD14* for myeloid cells, *CD79A* for B cells, *ALB* for hepatocytes, and *PLVAP* and *ACTA2* for stromal cells (Fig. 1C).[16,17] Cellular distribution in a uniform manifold approximation and projection (UMAP) plot indicated low batch effects between patients from the two original datasets (Fig. S1A). Significant differences in the transcriptomic profiles of hepatocytes, lymphocytes, and myeloid cells were observed between tumors and peritumoral regions, indicating their significant roles in HCC (Figs. S1B and C).

Next, we selected the hepatocyte partition from the tumor samples to analyze CSC. Reclustering of the hepatocytes identified eight functional clusters (Fig. 1D): HCC_CSC; HCC_ECM (extracellular matrix); HCC_Immune; HCC_Metabolism; HCC_Oncogene; HCC_Replication; HCC_Secretion; and HCC_Stress. The identities of these functional subclusters were confirmed through the analysis of differentially expressed genes (DEGs) (Fig. 1E). Considering the significance of CSCs in tumorigenesis and progression,[6] we focused on HCC_CSC for further investigations. Apart from the selective expression of CSC markers (Fig. 1E),[17,18] the HCC_CSC subpopulation also exhibited selective high expression of CSC signature epigenetic regulators (Fig. S1D),[19] transcription factors (TFs) (Fig. S1E),[19] and activation of stemness-related signaling pathways (Fig. S1F).[19] Taken together, these results validated the stemness of the HCC_CSC cluster.

Notably, although CSCs were functionally identified as a whole, the HCC_CSC cluster in fact comprised two transcriptionally distinct subclusters (Fig. 1F). To further characterize these two subclusters, we independently screened these subclusters for DEGs, and performed signaling pathway enrichment analysis. The results revealed activation of the Hippo signaling pathway (Fig. 1G, red box) and a signaling pathway regulating stem cell pluripotency (Fig. 1H, red box) in the DEGs from these two subclusters. This finding further confirms the stemness of these two subclusters.

Transcriptional characteristics and prognostic significance of CSC-like cells

To illustrate the transcriptomes of the CSC subclusters, we compared their gene expression profiles, identifying substantial DEGs between them (Fig. 2A). These subclusters were distinguished by different marker genes. One subcluster showed selective expression of *EPCAM*, *PROM1*, *TACSTD2*, *KRT19*, and *CD24*, whereas the other showed selective expression of *CD24* and *ICAM1* (Fig. 2B). Therefore, we designated these subclusters as CSC-conventional (CSC-con) and CSC-like cells, respectively.

The presence of CSC-like cells in tumors was further confirmed through multiplex immunofluorescence staining (Fig. 2C). Compared with the well-documented CSC-con, the CSC-like population remained obscure. Subsequently, we screened the DEGs of CSC-like cells for potential marker genes, identifying five additional genes: *ACSL4*, *GOLGA8B*, *C17orf67*, *BAG3*, and *RBM26* (Fig. 2D). Notably, these genes have been reported to be involved in cell stemness,[20–24] further supporting the stemness of CSC-like cells. Using HCC specimens, we confirmed the high levels of these genes in CSC-like cells (Fig. 2E and S2A). Compared with the CSC-con ($CD24^{+}ICAM1^{-}$) and non-CSC ($CD24^{-}$) subpopulations, the CSC-like ($CD24^{+}ICAM1^{+}$) subpopulation in both samples showed higher levels of *ACSL4*, *C17orf67*, and *BAG3* (Fig. 2F and S2B).

To validate the existence of CSC-like cells in a large number of patients with HCC, we performed bioinformatic analyses on three additional HCC cohorts, designated as cohort 3,[25] cohort 4,[26] and cohort 5[27] (Table S1). Following similar analysis procedures as used above, we identified CSC-like subpopulations in these cohorts and observed specific expression of CSC-like cell markers (Fig. 2G and S2C,D). Moreover, ACSL4 and BAG3

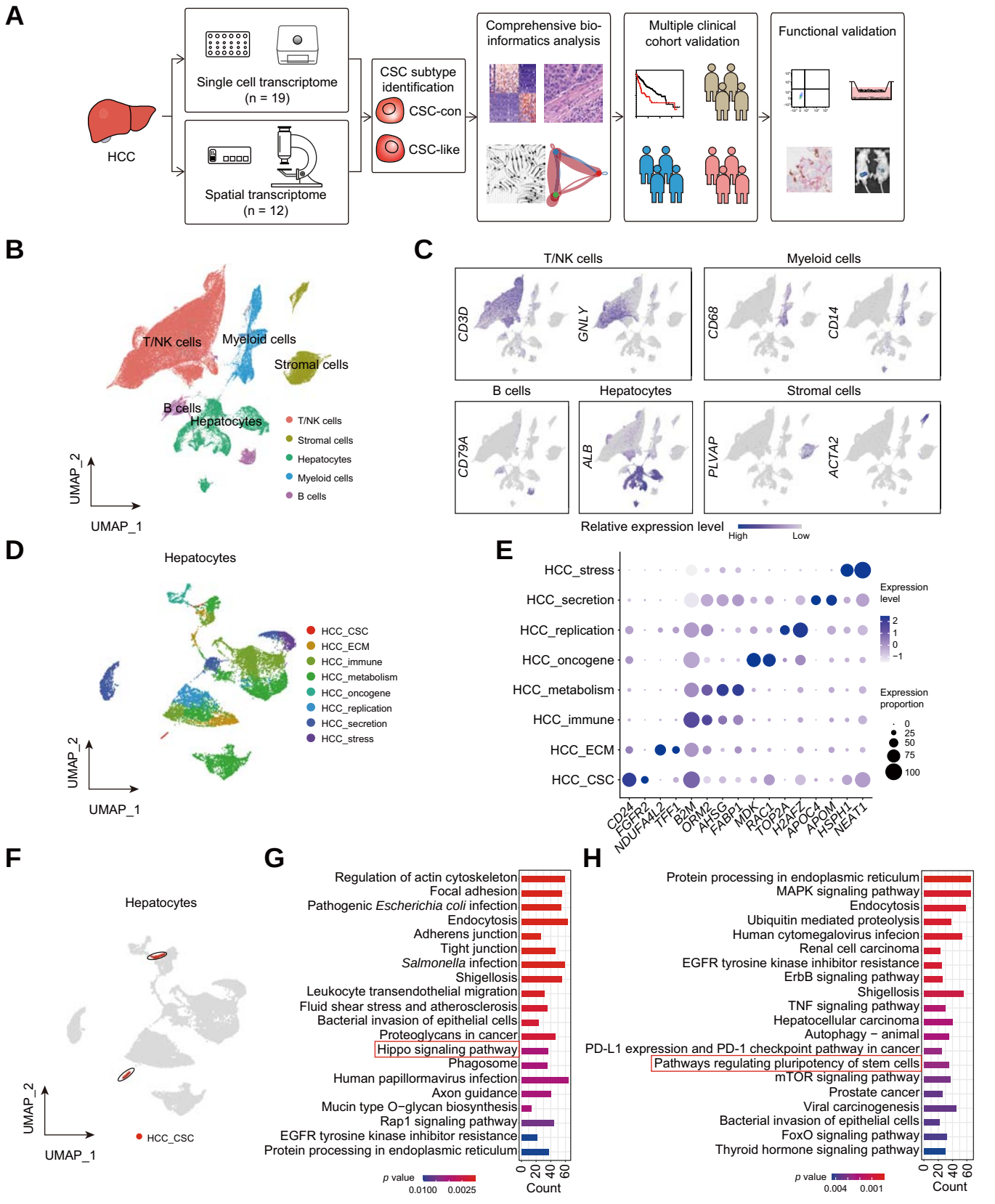

Fig. 1. Identification of CSC-like subclusters in HCC. (A) Schematic overview of the study design. (B) UMAP plot of integrated HCC scRNA-seq datasets. (C) Feature plots showing expression levels and distribution characteristics of marker genes for each partition. (D) UMAP plot displaying the functional clusters of HCC tumor cells. (E) Dot plot showing the marker gene expression levels of functional clusters in tumor cells. (F) UMAP plot visualizing CSC-con and CSC-like subclusters in HCC tumor cells. (G, H) Top 20 enriched signaling pathways of highly expressed genes in CSC-con (G) and CSC-like (H) subclusters. Stemness-related pathways are highlighted with red boxes. CSC, cancer stem cell; CSC-con, CSC-conventional; HCC, hepatocellular carcinoma; scRNA-seq, single cell RNA-sequencing; UMAP, uniform manifold approximation and projection.

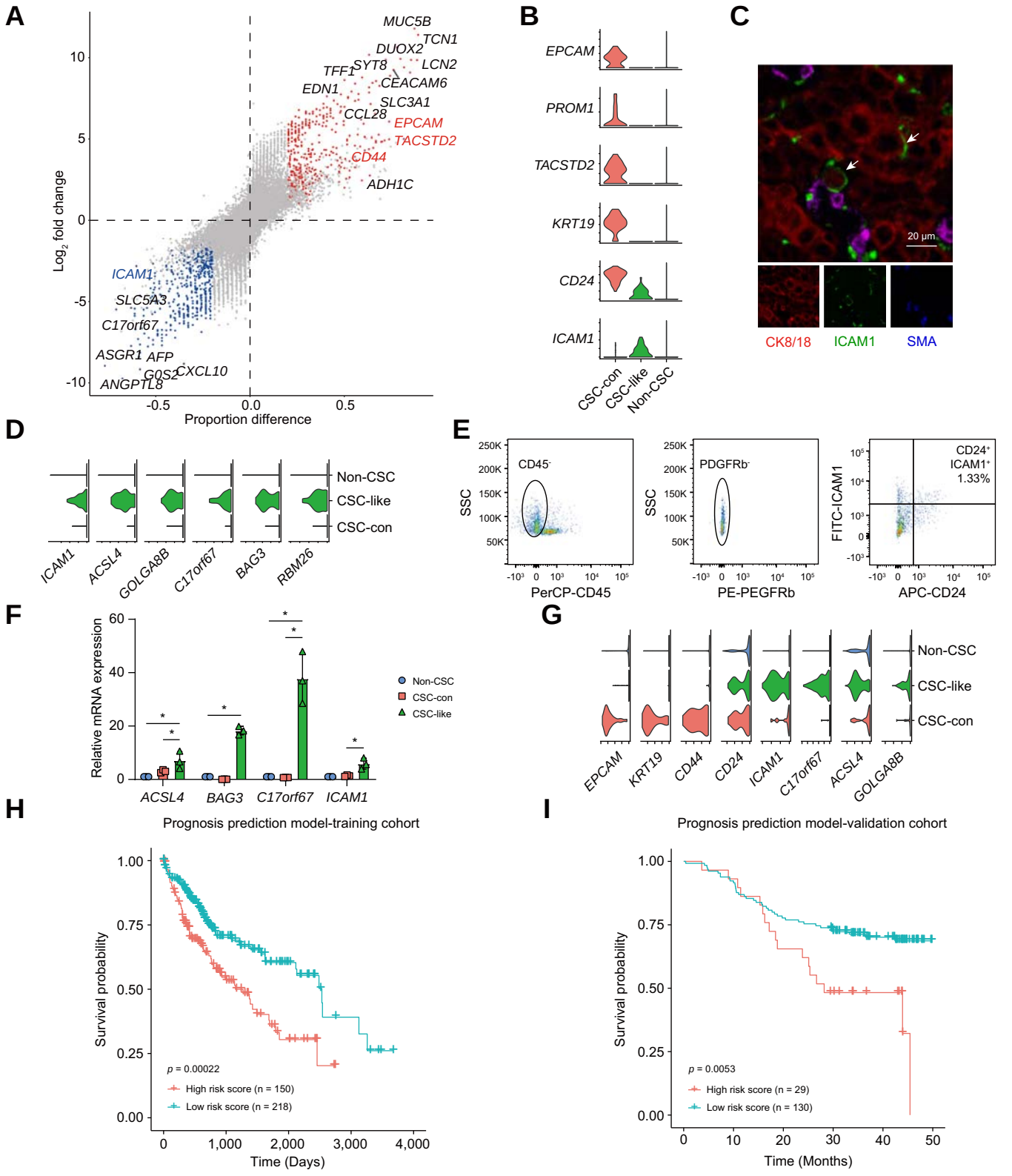

Fig. 2. Marker gene identification and prognosis evaluation of CSC-like cells. (A) DEG analysis comparing CSC-con (upper right) and CSC-like cells (below left). Dots and labels colored red, blue, and gray show the preferential gene expression in CSC-con, CSC-like, and no significant difference, respectively, between the two CSC subclusters. (B) Violin plots showing relative gene expression levels of CSC marker genes in CSC-con, CSC-like, and non-CSC cells. (C) Multiplex immunofluorescence staining of HCC samples highlighting CSC-like cells (indicated by white arrows for CK8/18^{+}SMA^{-}ICAM1^{+} cells). CK8/18 marks HCC tumor cells and SMA marks fibroblasts. (D) Violin plots showing relative gene expression levels of CSC-like marker genes in CSC-con, CSC-like, and non-CSC cells. (E) Flow cytometry analysis confirming the existence of CSC-like cells in an HCC sample. (F) qRT-PCR detecting expression levels of *ACSL4*, *BAG3*, *C17orf67*, and *ICAM1* in CSC-con, CSC-like, and non-CSC cells from an HCC sample. Unpaired Student *t* test: **p* <0.05, ***p* <0.01. (G) Relative expression levels of CSC-con markers (*EPCAM*, *KRT19*, *CD44* and *CD24*) and CSC-like cell markers (*CD24*, *ICAM1*, *C17orf67*, *ACSL4*, and *GOLGA8B*) in HCC tumor cell subclusters in cohort 3. (H) Survival analysis of

were also validated as CSC-like cell markers at the protein level (Fig. S2E) (cohort 6, Table S1).

To investigate the clinical significance of CSC-like cells, we detected the correlation between CSC-like cell markers and the prognosis of patients with HCC. We first analyzed the relationship between the expression levels of CSC-like cell-specific genes and HCC prognosis using clinical data from The Cancer Genome Atlas (TCGA) Program (cohort 7, Table S1). The results showed that CSC-like cell signature genes, including *CD24, ICAM1, ACSL4, BAG3, C17orf67, GOLGA8B*, and *RBM26*, were effective independent predictors of poor HCC prognosis (Fig. S2F).

To comprehensively evaluate HCC prognosis based on CSC-like cell abundance, we applied the least absolute shrinkage and selection operator (LASSO) regression algorithm to establish a prognostic evaluation model: HCC prognosis risk score = $0.059 \times Expr_{CD24} + 0.035 \times Expr_{ICAM1} + 0.083 \times Expr_{BAG3} + 0.030 \times Expr_{C17orf67} + 0.133 \times Expr_{RBM26}$. The prognosis evaluation model outperformed the single signature gene model (Fig. S2G). Patients with a higher risk score had significantly worse prognosis (Fig. 2H). We verified the prognostic prediction model using data from HCC cohort 8 (Table S1).[28] This resulted in validation of the prognostic prediction model at the protein level, with patients showing higher risk scores exhibiting significantly shorter survival periods compared with those with lower risk scores (Fig. 2I). These findings suggest that CSC-like cells are robust predictors of poor HCC prognosis at both the RNA and protein levels.

Cell invasiveness phenotype of CSC-like cells

To explore the functions of CSC-like cells in HCC development, we compared the enrichment of DEGs between CSC-con and CSC-like cells in an epithelial cell proliferation-related gene set, and observed significant enrichment of CSC-con DEGs in this gene set (Fig. S3A). Compared with the highly proliferative CSC-con, CSC-like cells exhibited a quiescent phenotype (Fig. S3B), suggesting distinct roles for CSC-like cells beyond cell proliferation. Next, we analyzed the stemness-related signaling pathways between CSC-con and CSC-like cells, and observed greater activation of JNK/MAPK signaling in CSC-like cells compared with CSC-con cells (Fig. 3A). In addition to its stemness-related roles, the JNK/MAPK signaling pathway has also been implicated in regulating cell metastasis.[29] Accordingly, we found enrichment of CSC-like DEGs in multiple metastasis-associated signaling pathways (Fig. 3B). Moreover, compared with CSC-con, CSC-like cells showed higher expression levels of mesenchymal-associated signature genes, including *ZEB1*, *FN1*, *GPC6*, *HTRA1*, and *CALD1* (Fig. 3C). Higher expression of these mesenchymal signature genes in CSC-like cells compared with CSC-con cells was also observed in HCC cohorts 3 (Fig. 3D) and 4 (Fig. 3E), indicating the enhanced metastatic potential of CSC-like cells.

To further verify the invasiveness of CSC-like cells, we detected the marker gene expression levels of CSC-con and CSC-like cells in circulation tumor cells (CTCs) of HCC (cohort 9, Table S1).[30] These CTCs are considered to be one of the most frequent origins of HCC metastasis. Therefore, the higher expression levels of CSC-like markers, rather than of CSC-con markers, indicated the enrichment of CSC-like cells in CTCs and their critical roles in HCC metastasis (Fig. 3F). Moreover, we observed a higher proportion of CSC-like cells in primary tumors with metastasis compared with those without metastasis in cohort 7 (Fig. 3G), further supporting the metastatic-promoting functions of CSC-like cells.

The high invasiveness of CSC-like cells was further validated using HCC samples and a mouse model. CSC-like cells sorted from HCC samples exhibited elevated *HTRA1* expression levels compared with non-CSC cells (Fig. 3H and S3C). Similarly, CSC-like cells sorted from the HCC cell line PLC/PRF/5 (Fig. S3D) showed greater *in vivo* metastatic potential compared with non-CSC cells (Fig. 3I and S3E,F). Collectively, these findings suggest the high invasiveness of CSC-like cells.

To elucidate the mechanisms underlying the invasiveness of CSC-like cells, we used SCENIC to explore the TFs. *CEBPG*, *NR3C1*, *CEBPA*, *DDIT3*, *ATF3*, *BCLAF1*, *JUN*, *NR2F6*, and *CHD2* were selectively activated in CSC-like cells (Fig. S3G). Among these TFs, *CEBPA* was predicted to be a TF of *CALD1* (a representative mesenchymal gene),[31] supporting the metastasis-promoting function of CSC-like cells. In conclusion, CSC-like cells represent a highly invasive subpopulation of CSCs in HCC.

Spatial distribution characteristics of CSC-like cells

To further investigate the histological characteristics of CSC-like cells, we analyzed the HCC microenvironments using ST. ST was performed on 12 fresh-frozen tumor specimens (cohort 10, Table S1) from patients with HCC (Table S3), and these tumor samples were classified based on their invasiveness. According to the completeness of the tumor capsules and the severity of intrahepatic spread, all 12 samples were classified into one of three types (Fig. 4A and S4). Tumors with an intact capsule were classified as type 1, comprising samples H4, H8, H9, H11, and H14 (Fig. 4A, yellow box). Type-2 tumors were characterized by incomplete capsules and the absence of intrahepatic spread, including samples H1, H2, H3, H12, and H13 (Fig. 4A, orange box). Type-3 tumors lacked complete capsules and exhibited intrahepatic disseminated foci, represented by samples H7 and H10 (Fig. 4A, red box). Spot clustering results from ST data revealed a perfect correspondence between the H&E staining (Fig. 4A [first lane] and S4A) and the spot annotation outcomes (Fig. 4A [second lane] and S4B). Signature gene analyses were used to confirm the annotations (Fig. 4A [third lane] and S4C). Furthermore, copy number variation (CNV) analysis of the ST subclusters identified significant CNV in the tumor regions (Fig. 4A [last lane] and S4D), further supporting the ST annotation results.

We next used SPOTlight analysis to map the spatial distribution of CSCs by integrating scRNA-seq and ST data. When analyzed according to tumor sample type, both CSC-con (Figs. S5A and B) and CSC-like cells (Fig. 4B and S5C) were

patients with HCC (cohort 7) showing survival correlation between prognosis risk score and RNA expression levels of CSC-like cell markers, Log-rank (Mantel-Cox) test. (I) Survival analysis of patients with HCC (cohort 8) showing correlation between prognosis risk score and protein expression levels of CSC-like cell markers, Log-rank (Mantel-Cox) test. CSC, cancer stem cell; CSC-con, CSC-conventional; DEG, differential gene expression; HCC, hepatocellular carcinoma.

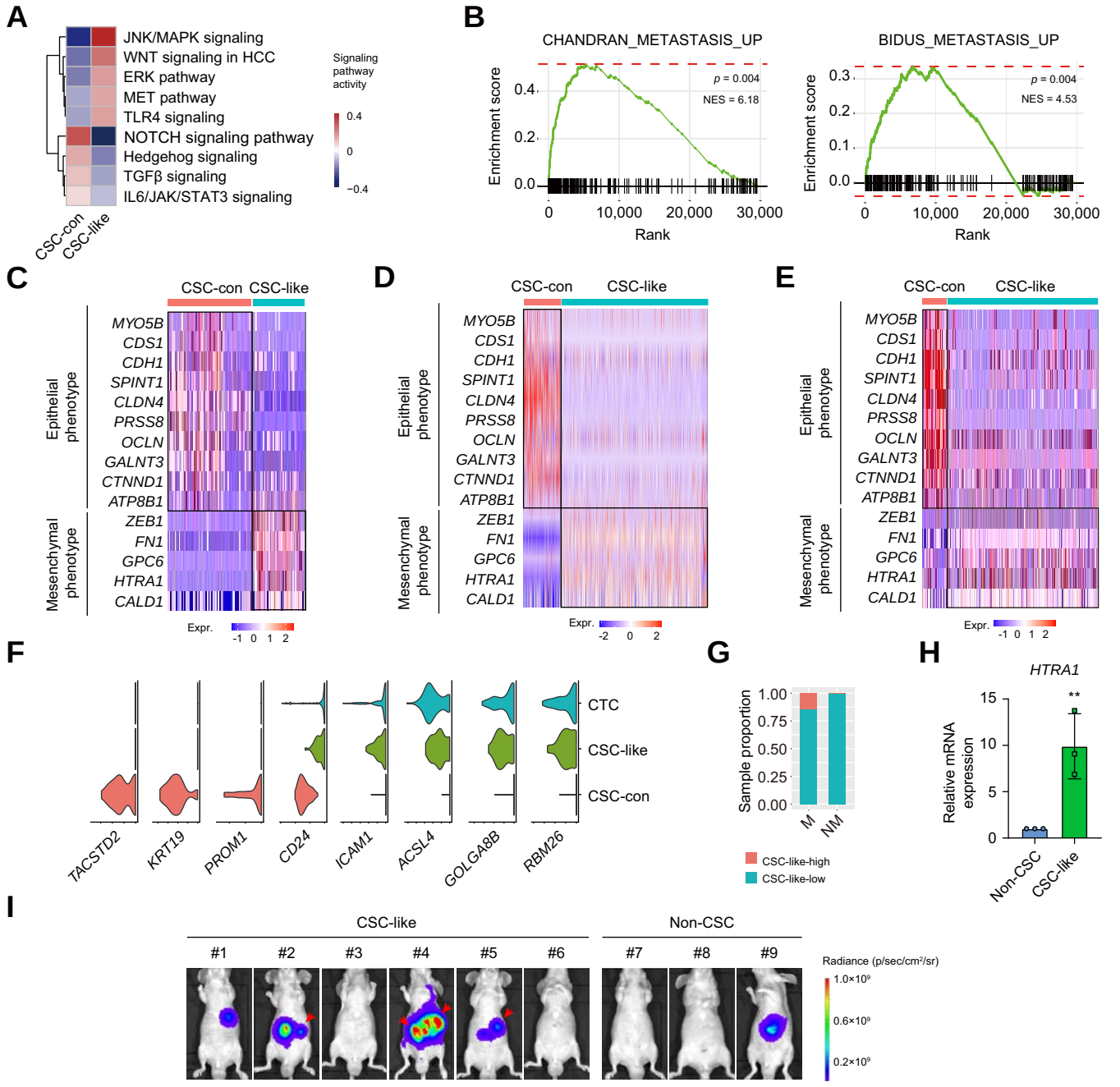

Fig. 3. Cell invasiveness of CSC-like cells. (A) Heatmap comparing the activity of typical CSC signaling pathways between CSC-con and CSC-like cells. (B) Gene set enrichment analysis plots showing the enrichment of CSC-like DEGs in cell metastasis signaling pathways. *p* values and normalized enrichment score are indicated. (C–E) Heatmaps showing differential expression levels of epithelial and mesenchymal genes in CSC-con and CSC-like cells in (C) the scRNA-seq data, (D) cohort 3, (E) and cohort 4. (F) Violin plots showing the relative expression levels of CSC marker genes in CTC from cohort 9 compared with CSC-con and CSC-like cells from our data. (G) Stacked histogram showing the CSC-like cell proportion in patients with HCC with (M) or without (NM) tumor metastasis in cohort 7. (H) qRT-PCR analysis of *HTRA1* expression levels in non-CSC versus CSC-like cell sorted from the HCC sample described in Fig. 2E: unpaired Student *t* test: ***p* <0.01. (I) *In vivo* bioluminescence imaging of nude mice injected intrahepatically with luciferase-labeled CSC-like cells or non-CSC cells at 7 weeks after cell injection. Red arrows indicate the intrahepatic disseminated foci. CSC, cancer stem cell; CSC-con, CSC-conventional; CTC, circulation tumor cell; DEG, differential gene expression; HCC, hepatocellular carcinoma; scRNA-seq, single-cell RNA sequencing.

more abundant in type-2 and type-3 HCC samples compared with type 1, suggesting a higher proportion of CSCs in aggressive tumors. Furthermore, type-3 HCC samples exhibited an abundance of CSC-like cells compared with type-2 HCC samples (Fig. 4B). In particular, *in situ* analysis revealed that CSC-like cells were more localized to metastasis sites rather than to primary tumor sites in both H7 (Fig. 4C) and H10 (Fig. 4D), indicating the involvement of CSC-like cell in tumor metastasis. Immunohistochemical (IHC) staining further validated the distribution feature of CSC-like cells, revealing

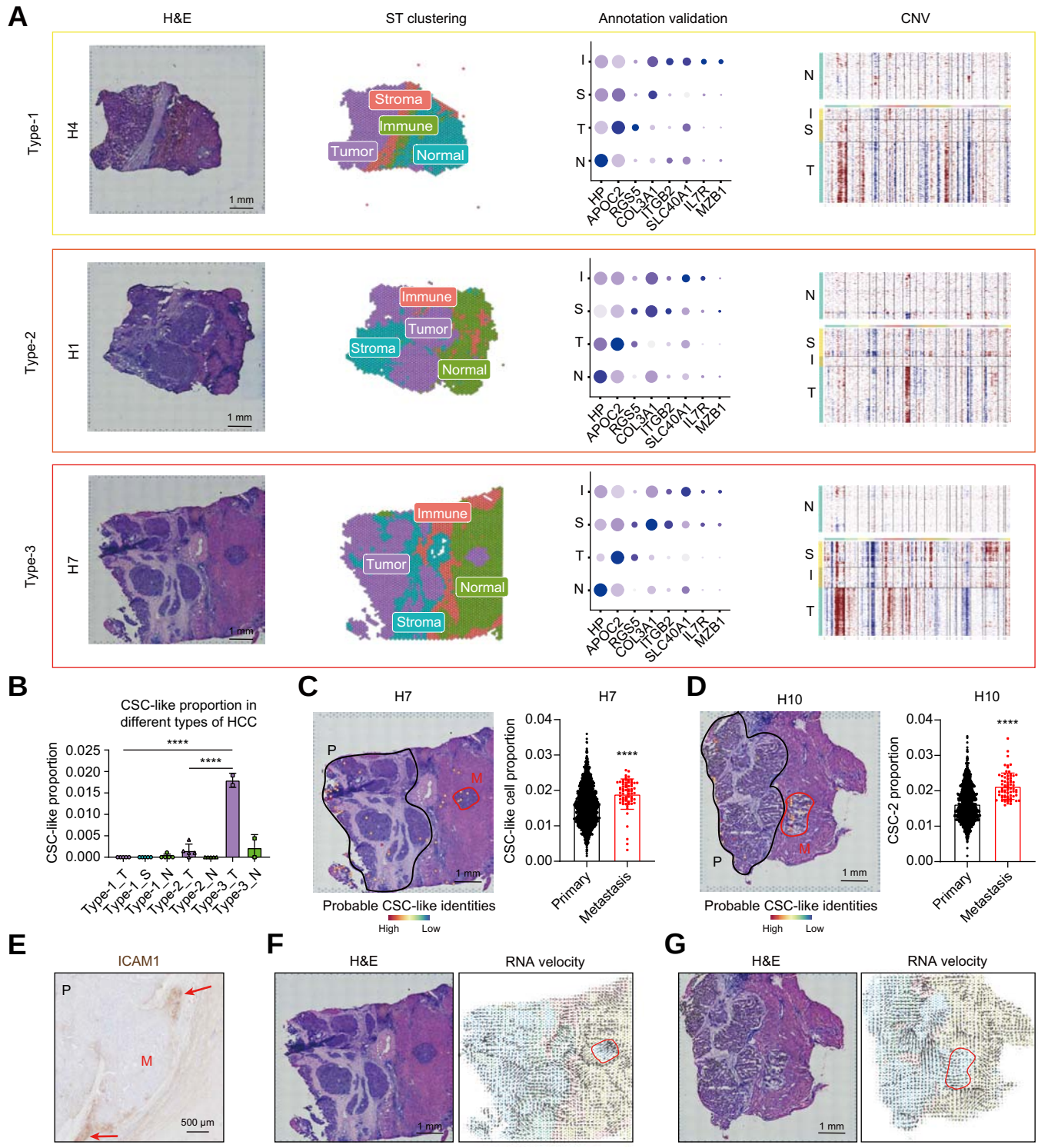

Fig. 4. Histopathological characteristics of CSC-like cells by ST data analysis. (A) Histopathological subtypes of HCC samples revealed by ST analysis. H&E staining (first lane), spot clustering results (second lane), marker gene expression levels (third lane), and CNV analysis (last lane) of ST data from HCC samples of H4 (type 1, yellow box), H1 (type 2, orange box), and H7 (type 3, red box). 'T' represents tumor tissue (indicated by *APOC2*); 'S' represents stroma (indicated by *RGS5* and *COL3A1*); 'N' represents peritumoral normal tissue (indicated by *HP*); and 'I' represents immune components (indicated by *ITGB2*, *SLC40A1*, *IL7R*, and *MZB1*). (B) Comparison of the relative proportion of CSC-like cells in tumor regions of type-1 (circles), type-2 (triangles), and type-3 (squares) HCC samples; unpaired Student *t* test: ****p <0.0001. (C, D) Histopathological distribution (left) and statistical analysis (right) of CSC-like cell abundance in H7 (C) and H10 (D). Primary tumors and metastasis foci are indicated by black and red circles, respectively; unpaired Student's *t* test: ****p <0.0001. (E) IHC staining showing the histopathological distribution of ICAM1 in primary and metastasis regions. Red arrows indicate the enrichment of ICAM1 protein in the tumor invasive frontline. (F, G) RNA velocity of H7 (F) and H10 (G). Arrows indicate directional cell state transition, with red circles highlighting intrahepatic disseminated foci. CSC, cancer stem cell; HCC, hepatocellular carcinoma; M, metastasis; P, primary; ST, spatial transcriptomics.

remarkable enrichment of ICAM1 expression at the tumor invasive frontline (Fig. 4E, red arrows).

To further confirm the localization of CSC-like cell in metastases, we analyzed RNA velocity *in situ*. In both H7 (Fig. 4F) and H10 (Fig. 4G) samples from our ST data, the evolution trajectory was directed from tumor disseminated foci, suggesting the enrichment of CSC-like cells in metastasis sites. Collectively, CSC-like cells exhibited preferential distribution in tumor metastasis sites.

Cellular interaction between CSC-like cells and tumor immune microenvironments

To explore the *in situ* functional mechanisms of CSC-like cells, we analyzed the cellular interaction network using CellChat. The clustering analysis of CSC-related signaling pathways identified four functional subgroups (Groups 1–4) (Fig. 5A). Signaling pathways in groups 1, 3, and 4 were functionally enriched in immunomodulatory pathways, including T cells, NK cells, dendritic cells (DCs), and macrophage activation pathways, indicating frequent interactions between CSCs and the tumor immune microenvironments (TIMEs) (Fig. 5B). Notably, CSC-like cells showed a distinct cellular interaction network compared with CSC-con (Fig. 5C). These signaling pathways were enriched in immune recruitment and chemokine-mediated cellular responses (Fig. 5D), further supporting the interactions between CSC-like cells and TIMEs. To visualize these interactions *in situ*, we resolved the cellular composition within CSC-like-positive spots in ST chips. The results showed a high abundance of immune cells, including myeloid cells and T/NK cells, within the CSC-like niche (Fig. 5E), indicating colocalization of CSC-like cells with immune cells and their cellular interactions.

To elucidate the exact cellular subtypes interacting with CSC-like cells, we reclustered the cell partitions in TME. Reclustering of myeloid cells resulted in 16 subclusters (Figs. S6A and B). Reclustering of stromal cells resulted in 21 subclusters (Figs. S6C and D), and that of lymphocytes resulted in 12 subclusters (Figs. S6E and F).

Immunosuppressive microenvironment induced by CSC-like cells

Next, we identified the distinct cell interactions of CSC-like cells by comparing the CellChat analysis results of CSC-con and CSC-like cells. In contrast to CSC-con cells, CSC-like cells exhibited selective activation of the ICAM signaling pathway (Fig. 6A). Components of the ICAM pathway comprised the ligand ICAM1 and various receptors, including SPN, ITGAL, ITGAX/ITGB2, ITGAM/ITGB2, and ITGAL/ITGB2 (Fig. S7A). Given the abundance of receptor pairs in macrophages and T cells (Fig. S7A), we hypothesized that CSC-like cells regulate the TME via macrophages and T cells. Among the macrophage subclusters, Macro_1, and Macro_4 exhibited the strongest interaction with CSC-like cells in the ICAM signaling pathway (Fig. 6B). M2 polarization of macrophages has been reported following ICAM1 signaling pathway activation.[32,33] Consistently, we observed M2-polarization phenotypes in these macrophage subclusters, evidenced by high expression levels of *MRC1*, *IL10*, and *TGFB1* (Fig. 6C). In addition, elevated expression levels of *SLC40A1*, *TREM2*, and *APOE*[34] were observed in Macro_1 and Macro_4 (Fig. S7B), further confirming the M2 polarization of these subclusters. High expression levels of these M2-polarization markers and ICAM1 receptors were specifically found in tumor regions rather than in peritumoral normal regions at the protein level (cohort 6, Table S1 and Fig. S7C), indicating the tumor-promoting function of this signaling pathway. Interestingly, CSC-like cells also displayed selective interaction with subclusters T cell_2, T cell_5, and T cell_6 (Fig. 6B). These T cell subclusters were characterized by high expression of *CTLA4*, *PDCD1*, *HAVCR2*, *LAG3*, and *TIGIT* (Fig. 6D). Hence, the enrichment of these immune checkpoint molecules[35] in CSC-like cell-interacting T cell subclusters offered direct evidence supporting the immunosuppressive states in the CSC-like niche.

We next investigated ICAM1 signaling histologically by reanalyzing the ST data. In specimens containing CSC-like cells (H1, H3, H7, H10, H12, and H13), we observed co-expression of *ICAM1* with *ITGB2*, *ITGAL*, and *ITGAM* in the same or adjacent spots on the ST chips (Fig. 6E,F and S7D), indicating activated ICAM1 signaling in the TME. The adjacent histological distribution of CSC-like cells (ICAM1-positive cell) with M2-polarized macrophages (CD163-positive cells) and CSC-like cells (ICAM1-positive cell) with exhausted T cells (PD-1-positive cells) was further confirmed through IHC staining (Fig. 6G,H). Furthermore, the correlation between the expression of *ICAM1* and macrophage M2-polarization marker genes, such as *CD163* and *CD200R*, as well as T cell exhaustion marker genes, including *TIGIT*, *HAVCR2*, and *CTLA4*, was further confirmed in HCC cohort 7 (Fig. 6I and S7E and Table S1). Taken together, these findings show that CSC-like cells induce M2 polarization of macrophages and promote T cell exhaustion.

Modulation of TIME through regulation of ICAM1 signaling

To verify the cellular interaction between CSC-like cells and the TIME, we sorted CSC-like cells ($CD24^{+}ICAM1^{+}$) and non-CSCs ($CD24^{-}$) from the HCC cell line PLC/PRF/5, and co-cultured these cells with THP-1 cells (Fig. 7A). THP-1 cells co-cultured with CSC-like cells showed higher expression levels of M2-polarization marker genes, including *CD163* and *CD200R*, compared with those co-cultured with non-CSC (Fig. 7B), suggesting that CSC-like cells induce M2 polarization of macrophages. Similarly, co-culture of CSC-like cells or non-CSCs with Jurkat (Fig. 7C) revealed consistent results. Jurkat cells co-cultured with CSC-like cells showed higher expression levels of exhaustion marker genes, including *PDCD1* and *TIGIT*, compared with those co-cultured with non-CSCs (Fig. 7D), indicating that CSC-like cells promoted T cell exhaustion.

Given the immunoinhibitory function of CSC-like cells, we next explored whether this phenomenon could be reversed by repressing ICAM1 signaling. We suppressed ICAM1 expression in tumor cells using short hairpin (sh)RNA (Fig. 7E), and co-cultured these cells with THP-1 or Jurkat cells. As a result, the immunoregulatory role of CSC-like cells was attenuated following ICAM1 knockdown (Fig. 7F,G).

Collectively, our data identified a CSC-like subpopulation in HCC that promotes tumor metastasis through high

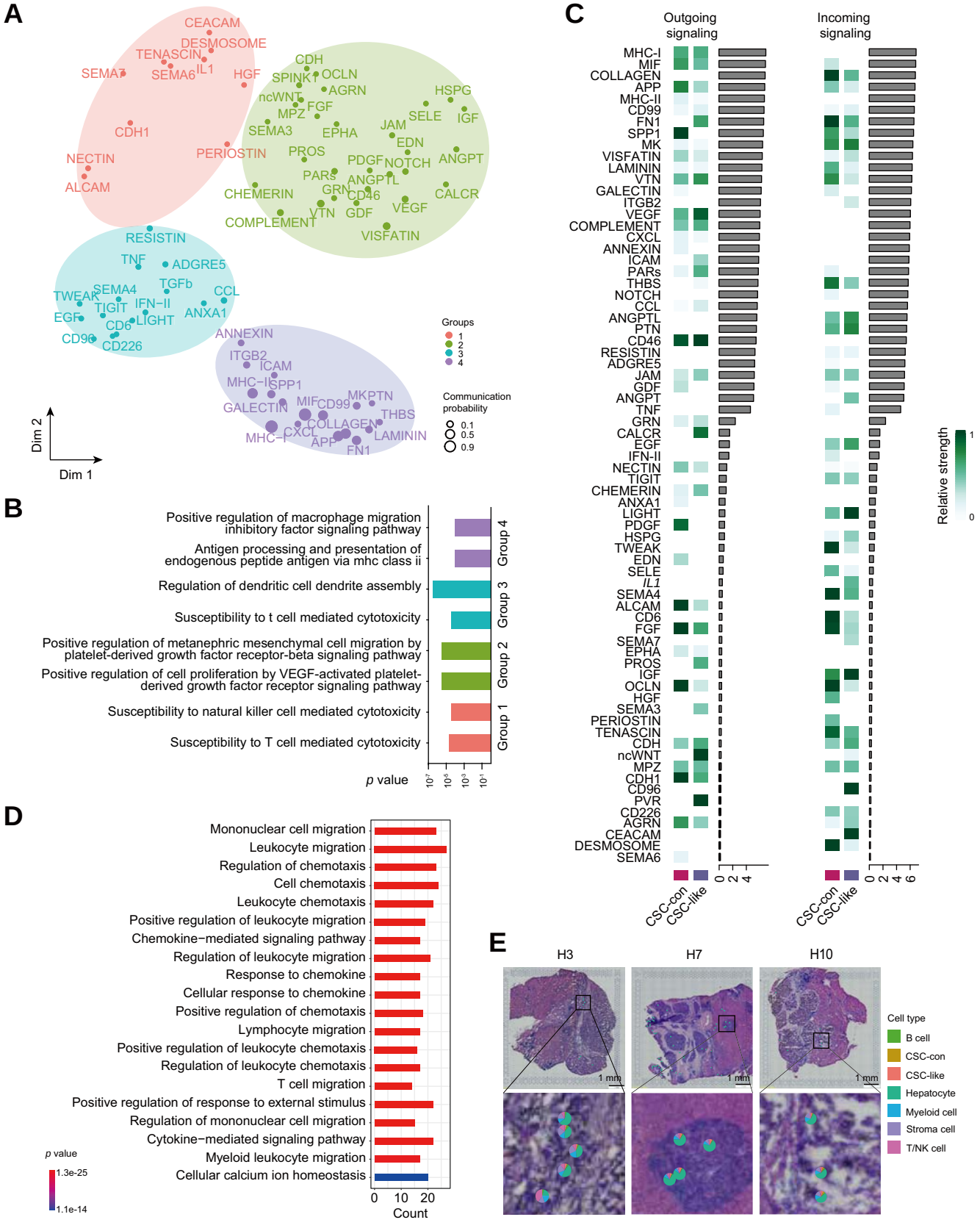

Fig. 5. Cellular interaction between CSC-like cell and tumor immune microenvironments. (A) Functional similarity analysis of activated signaling pathways in HCC_CSC cells. (B) Gene ontology analysis of pathways in the four groups identified in (A). (C) Heatmap comparing the relative signaling pathway strength between CSC-con and CSC-like cells. Interaction strength ranges from high (dark green) to low (white). Contribution to total outgoing or incoming signaling of each pathway is shown on the right. (D) Top 20 enriched signaling pathways of activated cellular interactions in CSC-like cells. (E) *In situ* distribution and cellular composition of CSC-like-positive spots in HCC samples of H3, H7, and H10. CSC, cancer stem cell; CSC-con, CSC-conventional; HCC, hepatocellular carcinoma.

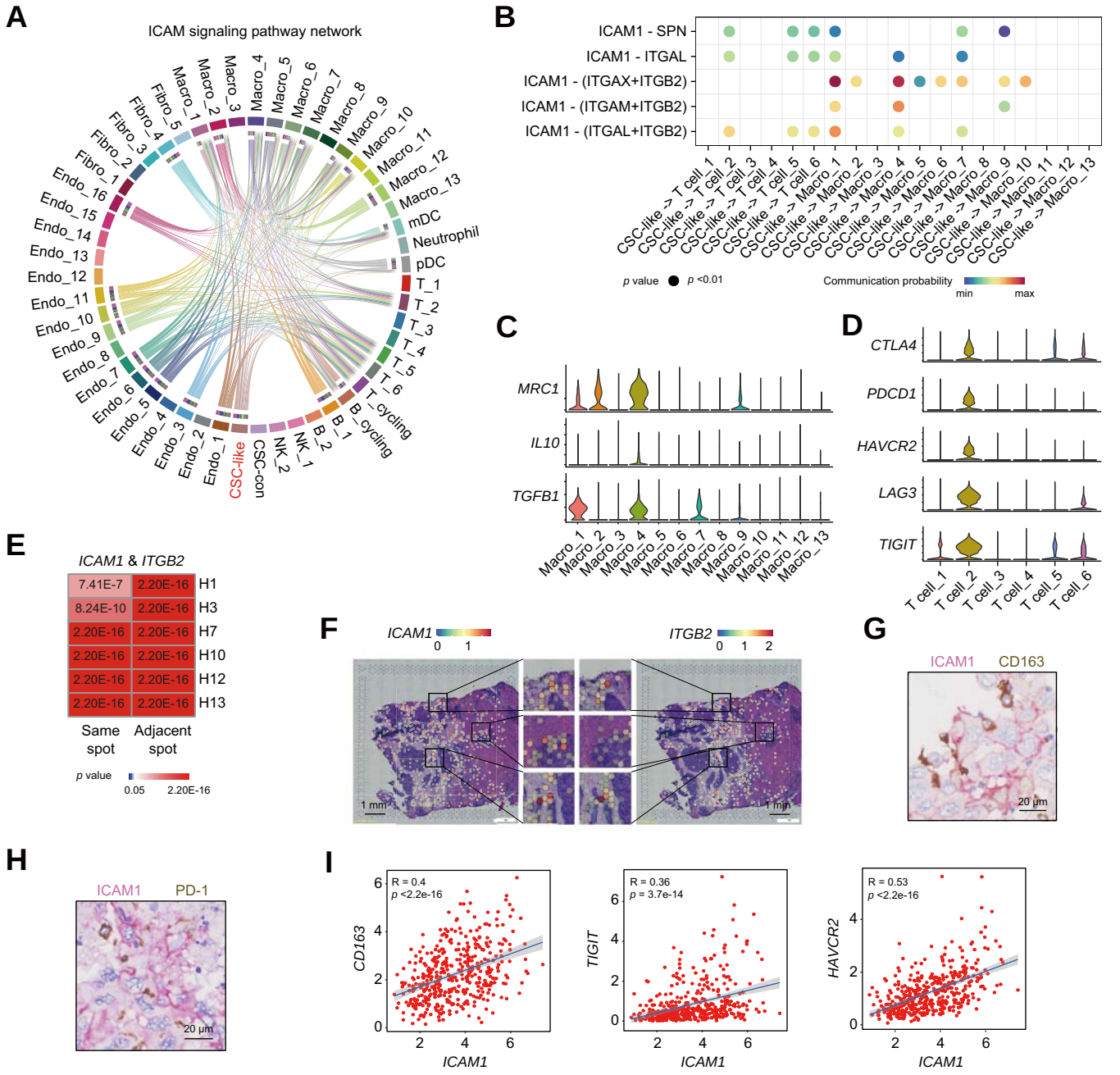

Fig. 6. Immunosuppressive microenvironment induced by CSC-like cells through the ICAM1 signaling pathway. (A) Chord diagram showing ICAM signaling pathway networks between the CSC-con, CSC-like cells, and HCC TME. (B) Bubble plot showing the communication probability of the ICAM pathway ligand–receptor pairs between subclusters of T cell, macrophage, and CSC-like cells. (C, D) Violin plots displaying the relative expression levels of (C) M2-polarization markers (*MRC1*, *IL10*, and *TGFB1*) in macrophage subclusters and (D) exhaustion markers (*CTLA4*, *PDCD1*, *HAVCR2*, *LAG3*, and *TIGIT*) in T cell subclusters. (E) Heatmap showing co-expression probabilities of *ICAM1*/*ITGB2* in the same or adjacent spots from HCC samples. Spearman's correlation analysis: *p* values of co-expression significance are colored from red ($p < 0.05$) to white ($p = 0.05$) and to blue ($p > 0.05$). (F) Distribution of *ICAM1* and *ITGB2* in the ST slide of HCC sample from H7. Zoomed-in portions of the HCC section (middle) show multiple areas of colocalization. (G, H) IHC double staining showing adjacent distribution of (G) CSC-like cells (ICAM1-positive) and M2-polarized macrophages (CD163-positive) and (H) CSC-like cells (ICAM1-positive) and exhausted T cells (PD-1-positive) in HCC. (I) Correlation analysis of the expression of *ICAM1* and immunosuppressive markers, including *CD163*, *TIGIT*, and *HAVCR2*, in cohort 7, Pearson's correlation analysis. CSC, cancer stem cell; CSC-con, CSC-conventional; HCC, hepatocellular carcinoma; IHC, immunohistochemistry; TME, tumor microenvironment.

invasiveness and regulation of TIME, driving it into immunosuppressive states. Furthermore, ICAM1 knockdown inhibited M2 polarization of macrophages and T cell exhaustion, thereby strengthening antitumor immune responses and repressing tumor metastasis (Fig. 7H).

Discussion

Although the heterogeneity of CSCs in HCC has been previously characterized using scRNA-seq and ST,[36–38] the functions of CSC subpopulations remain poorly understood. Our

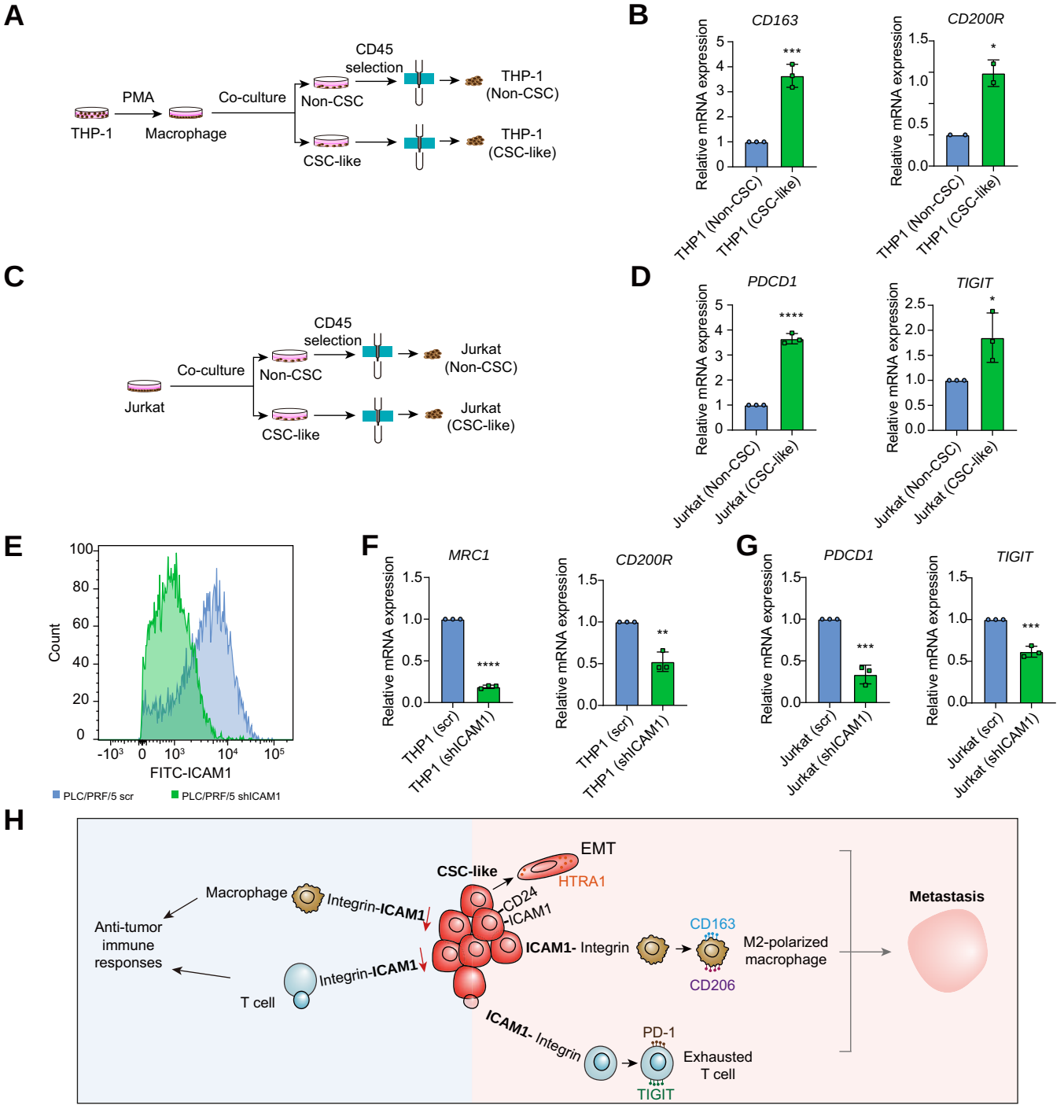

Fig. 7. Knockdown of *ICAM1* reverses the immunosuppression state of TME. (A) Schematic of the co-culture system of THP-1 cells with CSC-like cells and non-CSC cells. (B) qRT-PCR analysis of *CD163* and *CD200R* expression levels in THP1 cells co-cultured with CSC-like or non-CSC cells sorted from PLC/PRF/5; (C) Schematic of the co-culture system of Jurkat cells with CSC-like cells and non-CSC cells. (D) qRT-PCR analysis of *PDCD1* and *TIGIT* expression levels in Jurkat cells co-cultured with CSC-like or non-CSC cells sorted from PLC/PRF/5. (E) Flow cytometry confirming the downregulation of ICAM1 expression in PLC/PRF/5 shICAM1 cells. (F) qRT-PCR detection of *MRC1* and *CD200R* expression levels in THP1 cells co-cultured with sh-scramble (scr) or shICAM1 PLC/PRF/5 cells. (G) qRT-PCR detection of *PDCD1* and *TIGIT* expression levels in Jurkat cells co-cultured with sh-scramble (scr) or shICAM1 PLC/PRF/5 cells. (H) Schematic showing the functional mechanisms of CSC-like cells in tumor metastasis. CSC-like cells promote tumor metastasis through high invasiveness and immunosuppression roles via cellular interaction with macrophages and T cells via ICAM1 signaling. Knockdown of *ICAM1* in CSC-like cells reverses the suppressive TME and inhibits tumor metastasis. Unpaired Student *t* test: **p* <0.05, ****p* <0.001, *****p* <0.0001. CSC, cancer stem cell; IHC, immunohistochemistry; TME, tumor microenvironment.

study integrated scRNA-seq and ST data and identified CSC-like cells as the metastasis-promoting CSC subpopulation in HCC. CSC-like cells function in tumor metastasis through the following mechanisms. First, the CSC-like subpopulation exhibits high invasiveness by expressing high levels of epithelial–mesenchymal transition (EMT) signature genes. Second, CSC-

like cells induce macrophage M2 polarization and T cell exhaustion via the ICAM signaling pathway, reshaping the immune microenvironment into immunosuppressive states and permitting tumor metastasis. Intriguingly, CSC-like cell markers, including ICAM1, ACSL4, GOLGA8B, and BAG3, may provide additional potential mechanisms for the metastasis-promoting behavior of CSC-like cells. In HCC, high levels of ICAM1 in serum and tumor tissue have been shown to correlate with tumor metastasis[39,40]: ACSL4 reprograms fatty acid metabolism and induces tumor progression[41]; GOLGA8B regulates cell invasion and metastasis through the STAT3 signaling pathway[42]; and BAG3 locates at the leading edge of migrating cells and regulates EMT.[43] Collectively, these findings not only support the metastasis-promoting function of CSC-like cells, but also imply the involvement of more underlying mechanisms.

CSCs are highly involved in tumorigenesis and recurrence by definition,[44,45] making them ideal therapeutic targets. Numerous clinical trials are targeting CSC surface antigens.[46] However, the results of many CSC-targeted clinical trials have been disappointing because of severe side effects. Approximately one-third of patients participating in anti-CD44 or anti-ALK-1 (TGF-β receptor) clinical trials suffered severe adverse events.[47,48] These results are likely the result of the extensive similarities of normal stem cells and CSCs,[49] especially the CSC-con population. Therefore, targeting metastasis-specific CSC subpopulations, referred to as the CSC-like population, could offer novel insights into suppressing HCC progression. Hence, inhibitors targeting CSC-like cell markers, including ICAM1, C17orf67, ACSL4, GOLGA8B, BAG3, and RBM26, have the potential to suppress HCC progression without affecting normal stem cells, thereby significantly reducing side effects. Transformations between CSC-con and CSC-like cells should be considered when designing CSC-targeting drugs. Therefore, future investigations could focus on evaluating the plasticity of CSC subpopulations. Simultaneously targeting both CSC subpopulations could improve prognosis, while identifying key transformation regulators between CSC-con and CSC-like cells could provide new treatment strategies for HCC.

By comprehensive use of scRNA-seq and ST data, our study not only elucidates the gene expression profile and *in situ* cellular interactions of the CSC subpopulation, but also provides the first spatial maps of its distribution. Both CSC-con and CSC-like cells were more abundant in invasive tumors lacking intact capsules. Previous work highlighted the associations between tumor capsule and patient prognosis, including tumor metastasis and recurrence.[50] The widely accepted explanation for this phenotype is that the fibrotic structure forms a physical barrier against tumor migration, while our findings introduce a novel theory based on CSCs. Tumors can be classified into highly aggressive and less aggressive categories depending on their invasiveness. CSCs, especially CSC-like cells, are enriched in highly aggressive tumors and infiltrate stroma regions before the formation of thick capsules. These CSCs highjack immune cells and invade microvessels, ultimately driving tumor metastasis.

In conclusion, by integrating bioinformatics analyses of scRNA-seq and ST data, our study identifies a metastasis-promoting CSC subtype, referred to as CSC-like cells. This subpopulation is characterized by a high expression of CD24, ICAM1, ACSL4, GOLGA8B, C17orf67, BAG3, and RBM26, and shows strong metastatic potential. Spatially, CSC-like cells are enriched in invasive tumors, especially in metastatic sites. Functionally, CSC-like cells drive macrophage M2 polarization and T cell exhaustion, contributing to the establishment of an immuno-suppressive microenvironment. Thus, this metastasis-initiating CSC-like subpopulation represents a promising therapeutic target for HCC treatment.

Affiliations

[1]*Institute of Systems Biomedicine, Department of Pathology, Center of Basic Medical Research, Institute of Medical Innovation and Research, School of Basic Medical Sciences, Peking-Tsinghua Center for Life Sciences, Peking University Third Hospital, Peking University, Beijing 100191, China;* [2]*Institute of Precision Medicine, Peking University Shenzhen Hospital, Shenzhen 518036, China;* [3]*Faculty of Hepato-Pancreato-Biliary Surgery, Chinese PLA General Hospital, Beijing 100853, China;* [4]*Senior Department of Hepatology, Fifth Medical Center of Chinese PLA General Hospital, 100039 Beijing, China;* [5]*Department of Medical Genetics, School of Basic Medical Sciences Peking University, Beijing 100191, China*

Abbreviations

CNV, copy number variation; CSC-con, CSC-conventional; CSC, cancer stem cell; CTC, circulation tumor cell; DC, dendritic cells; DEG, differentially expressed gene; ECM, extracellular matrix; EMT, epithelial–mesenchymal transition; HCC, hepatocellular carcinoma; IHC, immunohistochemistry; LASSO, least absolute shrinkage and selection operator; LGR5, leucine-rich repeat-containing G-protein-coupled receptor 5; M, metastasis; NK, natural killer; P, primary; scr, sh-scramble; scRNA-seq, single-cell RNA sequencing; shRNA, short hairpin RNA; ST, spatial transcriptomics; TCGA, The Cancer Genome Atlas; TF, transcription factor; TIME, tumor immune microenvironment; TME, tumor microenvironment; UMAP, uniform manifold approximation and projection.

Financial support

This work was supported by grants including the National Key Research and Development Program of China (2021YFA1300601 to YY), National Natural Science Foundation of China (82030081 to YY, 30700349, 30440012 to LG, and 32101047 to YL), the Beijing Municipal Science and Technology Commission (Z131100004013036 to LG), the Shu Fan Education and Research Foundation, and the Lam Chung Nin Foundation for Systems Biomedicine.

Conflicts of interest

The authors declare no conflicts of interest that pertain to this work.

Please refer to the accompanying ICMJE disclosure forms for further details.

Authors' contributions

Conceived the study and designed major experiments: YY, LG, CY. Performed sample preparation: CY, YL, ZW, GW, YB, GL. Performed DNA library construction of scRNA-seq and ST sequencing: XM. Performed sample collection, clinical diagnosis, and evaluation of the validation study: LG, YB. Performed IHC: YL, LG. Performed the animal experiments: ZH, CY. Analyzed scRNA-seq data: CY, GZ, AL, YJ. Analyzed ST data: CY, GZ, XZhang. Performed flow cytometry and quantitative real-time PCR: CY, YL. Performed MS and analyzed the data: HS, XZhao. Wrote the manuscript: CY, JL, LG, YY. The first-author position is determined by the relative degree of contribution to this study.

Data availability statement

The raw data of scRNA-seq and ST results have been added to the Genome Sequence Archive for Human (https://ngdc.cncb.ac.cn/gsa-human/) under accession number HRA001399.

Acknowledgements

We thank Susan P.C. Cole for assistance with manuscript editing. We thank Dan Lu, Yichen Deng, and Xiaowei Tang for assistance with cell co-culture experiments, flow cytometry, and bioinformatic analyses, respectively. We thank Qi Yin, Xin Zhou, Yang Zheng, Sen Wang, and Peng Li for assistance with tumor sample preparation.

Supplementary data

Supplementary data to this article can be found online at https://doi.org/10.1016/j.jhepr.2024.101302.

References

Author names in bold designate shared co-first authorship

[1] Akinyemiju T, Abera S, Ahmed M, et al. The burden of primary liver cancer and underlying etiologies from 1990 to 2015 at the global, regional, and national level: results from the global burden of disease study 2015. JAMA Oncol 2017;3:1683–1691.
[2] Sung H, Ferlay J, Siegel RL, et al. Global Cancer Statistics 2020: GLOBOCAN estimates of incidence and mortality worldwide for 36 cancers in 185 countries. Ca: Cancer J Clin 2021;71:209–249.
[3] Llovet JM, Montal R, Sia D, et al. Molecular therapies and precision medicine for hepatocellular carcinoma. Nat Rev Clin Oncol 2018;15:599–616.
[4] Lee SK, Lee SW, Jang JW, et al. Immunological markers, prognostic factors and challenges following curative treatments for hepatocellular carcinoma. Int J Mol Sci 2021;22:10271.
[5] European Association for the Study of the Liver. EASL Clinical Practice Guidelines: management of hepatocellular carcinoma. J Hepatol 2018;69:182–236.
[6] Lytle NK, Barber AG, Reya T. Stem cell fate in cancer growth, progression and therapy resistance. Nat Rev Cancer 2018;18:669–680.
[7] Clara JA, Monge C, Yang Y, et al. Targeting signalling pathways and the immune microenvironment of cancer stem cells — a clinical update. Nat Rev Clin Oncol 2019;17:204–232.
[8] Min J, Zhang C, Bliton RJ, et al. Dysplastic stem cell plasticity functions as a driving force for neoplastic transformation of precancerous gastric mucosa. Gastroenterology 2022;163:875–890.
[9] **Fumagalli A**, **Oost KC**, Kester L, et al. Plasticity of lgr5-negative cancer cells drives metastasis in colorectal cancer. Cell Stem Cell 2020;26:569–578.e7.
[10] de Sousa e Melo F, Kurtova AV, Harnoss JM, et al. A distinct role for lgr5+ stem cells in primary and metastatic colon cancer. Nature 2017;543:676–680.
[11] Longo SK, Guo MG, Ji AL, et al. Integrating single-cell and spatial transcriptomics to elucidate intercellular tissue dynamics. Nat Rev Genet 2021;22:627–644.
[12] **Ji AL**, **Rubin AJ**, **Thrane K**, et al. Multimodal analysis of composition and spatial architecture in human squamous cell carcinoma. Cell 2020;182:497–514.e22.
[13] Moncada R, Barkley D, Wagner F, et al. Integrating microarray-based spatial transcriptomics and single-cell RNA-seq reveals tissue architecture in pancreatic ductal adenocarcinomas. Nat Biotechnol 2020;38:333–342.
[14] **Thrane K**, **Eriksson H**, Maaskola J, et al. Spatially resolved transcriptomics enables dissection of genetic heterogeneity in stage III cutaneous malignant melanoma. Cancer Res 2018;78:5970–5979.
[15] Sharma A, Seow JJW, Dutertre CA, et al. Onco-fetal reprogramming of endothelial cells drives immunosuppressive macrophages in hepatocellular carcinoma. Cell 2020;183:377–394.e21.
[16] Ramachandran P, Dobie R, Wilson-Kanamori JR, et al. Resolving the fibrotic niche of human liver cirrhosis at single-cell level. Nature 2019;575:512–518.
[17] Aizarani N, Saviano A, Sagar, et al. A human liver cell atlas reveals heterogeneity and epithelial progenitors. Nature 2019;572:199–204.
[18] Lee TK, Castilho A, Cheung VC, et al. CD24+ liver tumor-initiating cells drive self-renewal and tumor initiation through STAT3-mediated NANOG regulation. Cell Stem Cell 2011;9:50–63.
[19] Lee TK-W, Guan X-Y, Ma S. Cancer stem cells in hepatocellular carcinoma — from origin to clinical implications. Nat Rev Gastroenterol Hepatol 2021;19:26–44.
[20] **Li H**, **Song J**, He Y, et al. CRISPR/Cas9 screens reveal that hexokinase 2 enhances cancer stemness and tumorigenicity by activating the ACSL4-fatty acid β-oxidation pathway. Adv Sci 2022;9:e2105126.
[21] **Li X-Y**, **Yan J**, Sun J, et al. BAG3 deletion suppresses stem cell-like features of pancreatic ductal adenocarcinoma via translational suppression of ISG15. Biochim Biophys Acta Mol Cel Res 2019;1866:819–827.
[22] Im C-N, Yun H, Lee J-H. Heat shock factor 1 depletion sensitizes A172 glioblastoma cells to temozolomide via suppression of cancer stem cell-like properties. Int J Mol Sci 2017;18:468.
[23] Lako M, Pashai N, Hao H, et al. Genome-wide profiling of pluripotent cells reveals a unique molecular signature of human embryonic germ cells. PLoS One 2012;7:e39088.
[24] Sweef O, Yang C, Wang Z. The oncogenic and tumor suppressive long noncoding RNA–microRNA–messenger RNA regulatory axes identified by analyzing multiple platform omics data from cr(VI)-transformed cells and their implications in lung cancer. Biomedicines 2022;10:2334.
[25] **Sun Y**, **Wu L**, **Zhong Y**, et al. Single-cell landscape of the ecosystem in early-relapse hepatocellular carcinoma. Cell 2021;184:404–421.e16.
[26] **Zhu G-Q**, **Tang Z**, **Huang R**, et al. CD36+ cancer-associated fibroblasts provide immunosuppressive microenvironment for hepatocellular carcinoma via secretion of macrophage migration inhibitory factor. Cell Discov 2023;9:25.
[27] **Lu Y**, **Yang A**, **Quan C**, et al. A single-cell atlas of the multicellular ecosystem of primary and metastatic hepatocellular carcinoma. Nat Commun 2022;13:4594.
[28] **Gao Q**, **Zhu H**, **Dong L**, et al. Integrated proteogenomic characterization of HBV-related hepatocellular carcinoma. Cell 2019;179:561–577.e22.
[29] Kciuk M, Gielecińska A, Budzinska A, et al. Metastasis and MAPK pathways. Int J Mol Sci 2022;23:3847.
[30] **Sun YF**, **Wu L**, **Liu SP**, et al. Dissecting spatial heterogeneity and the immune-evasion mechanism of CTCs by single-cell RNA-seq in hepatocellular carcinoma. Nat Commun 2021;12:4091.
[31] ENCODE Project Consortium. An integrated encyclopedia of DNA elements in the human genome. Nature 2012;489:57–74.
[32] **Yin M**, **Li X**, **Tan S**, et al. Tumor-associated macrophages drive spheroid formation during early transcoelomic metastasis of ovarian cancer. J Clin Invest 2016;126:4157–4173.
[33] **Yu T**, **Gan S**, **Zhu Q**, et al. Modulation of M2 macrophage polarization by the crosstalk between Stat6 and Trim24. Nat Commun 2019;10:4353.
[34] **Zhang Q**, **He Y**, **Luo N**, et al. Landscape and dynamics of single immune cells in hepatocellular carcinoma. Cell 2019;179:829–845.e20.
[35] Thommen DS, Schumacher TN. T cell dysfunction in cancer. Cancer Cell 2018;33:547–562.
[36] **Zheng H**, **Pomyen Y**, Hernandez MO, et al. Single-cell analysis reveals cancer stem cell heterogeneity in hepatocellular carcinoma. Hepatology 2018;68:127–140.
[37] **Ho DW**, **Tsui YM**, Sze KM, et al. Single-cell transcriptomics reveals the landscape of intra-tumoral heterogeneity and stemness-related subpopulations in liver cancer. Cancer Lett 2019;459:176–185.
[38] **Wu R**, **Guo W**, **Qiu X**, et al. Comprehensive analysis of spatial architecture in primary liver cancer. Sci Adv 2021;7:eabg3750.
[39] Sun J-J, Zhou X-D, Liu Y-K, et al. Invasion and metastasis of liver cancer: expression of intercellular adhesion molecule 1. J Cancer Res Clin Oncol 1999;125:28–34.
[40] Zhu P-P, Yuan S-G, Liao Y, et al. High level of intercellular adhesion molecule-1 affects prognosis of patients with hepatocellular carcinoma. World J Gastroenterol 2015;21:7254–7263.
[41] **Chen J**, **Ding C**, **Chen Y**, et al. ACSL4 reprograms fatty acid metabolism in hepatocellular carcinoma via c-Myc/SREBP1 pathway. Cancer Lett 2021;502:154–165.
[42] Li Z, Li Y, Li N, et al. Silencing GOLGA8B inhibits cell invasion and metastasis by suppressing STAT3 signaling pathway in lung squamous cell carcinoma. Clin Sci 2022;136:895–909.
[43] Xiao H, Cheng S, Tong R, et al. BAG3 regulates epithelial–mesenchymal transition and angiogenesis in human hepatocellular carcinoma. Lab Invest 2014;94:252–261.
[44] Llovet JM, Kelley RK, Villanueva A, et al. Hepatocellular carcinoma. Nat Rev Dis Primers 2021;7:6.
[45] Lambert AW, Pattabiraman DR, Weinberg RA. Emerging biological principles of metastasis. Cell 2017;168:670–691.
[46] **Yang L**, **Shi P**, Zhao G, et al. Targeting cancer stem cell pathways for cancer therapy. Signal Transduct Target Ther 2020;5:8.
[47] Judd NP, Winkler AE, Murillo-Sauca O, et al. ERK1/2 regulation of CD44 modulates oral cancer aggressiveness. Cancer Res 2012;72:365–374.

[48] Simonelli M, Zucali P, Santoro A, et al. Phase I study of PF-03446962, a fully human monoclonal antibody against activin receptor-like kinase-1, in patients with hepatocellular carcinoma. Ann Oncol 2016;27:1782–1787.
[49] Trumpp A, Haas S. Cancer stem cells: the adventurous journey from hematopoietic to leukemic stem cells. Cell 2022;185:1266–1270.
[50] Shimbashi W, Sugitani I, Kawabata K, et al. Thick tumor capsule is a valuable risk factor for distant metastasis in follicular thyroid carcinoma. Auris Nasus Larynx 2018;45:147–155.

Keywords: Hepatocellular carcinoma; Single-cell RNA sequencing; Spatial transcriptomics; Cancer stem cell; Metastasis; Tumor microenvironment.

Received 27 August 2024; received in revised form 5 December 2024; accepted 10 December 2024; Available online 16 December 2024